

# RSC Advances

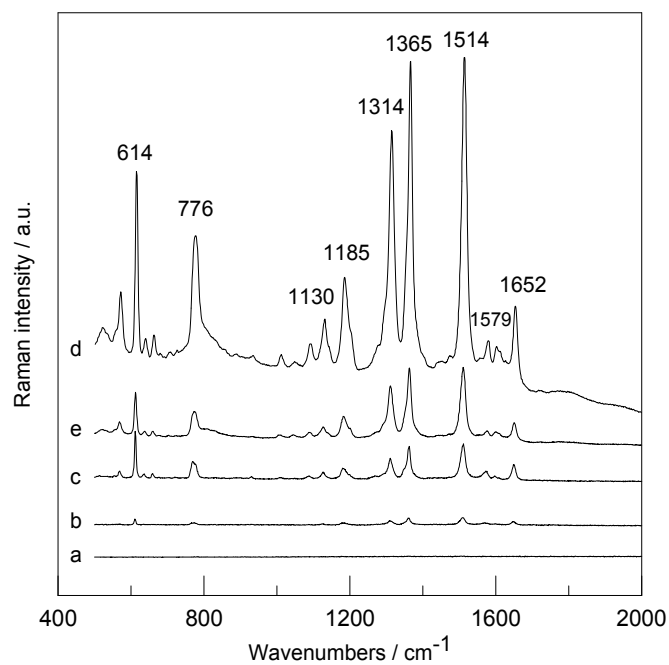


This is an *Accepted Manuscript*, which has been through the Royal Society of Chemistry peer review process and has been accepted for publication.

*Accepted Manuscripts* are published online shortly after acceptance, before technical editing, formatting and proof reading. Using this free service, authors can make their results available to the community, in citable form, before we publish the edited article. This *Accepted Manuscript* will be replaced by the edited, formatted and paginated article as soon as this is available.

You can find more information about *Accepted Manuscripts* in the [Information for Authors](#).

Please note that technical editing may introduce minor changes to the text and/or graphics, which may alter content. The journal's standard [Terms & Conditions](#) and the [Ethical guidelines](#) still apply. In no event shall the Royal Society of Chemistry be held responsible for any errors or omissions in this *Accepted Manuscript* or any consequences arising from the use of any information it contains.



SERS of R6G absorbed on this developed array exhibits a higher intensity by ca. 30-fold of magnitude, as compared with that of R6G absorbed on the Au NPs-based array without the modification of Ag films.

**Surface-enhanced Raman scattering on silver film-modified Au  
nanoparticles-decorated SiO<sub>2</sub> mask array**

Chi-Ching Chang<sup>a,b</sup>, Liang-Yih Chen<sup>c</sup>, Kuang-Hsuan Yang<sup>d</sup>, Qing-Ye Chen<sup>d</sup>, Yu-Chih  
Liang<sup>e</sup>, Shyr-Yi Lin<sup>f\*</sup> and Yu-Chuan Liu<sup>g,h\*</sup>

<sup>a</sup>Division of Rheumatology, Immunology and Allergy, Taipei Medical University Hospital,  
No. 252, Wuxing St., Taipei 11031, Taiwan

<sup>b</sup>Graduate Institute of Clinical Medicine, School of Medicine, College of Medicine, Taipei  
Medical University, No. 250, Wuxing St., Taipei 11031, Taiwan

<sup>c</sup>Department of Chemical Engineering, National Taiwan University of Science and  
Technology, No. 43, Sec. 4, Keelung Rd., Taipei 10607, Taiwan.

<sup>d</sup>Department of Materials Science and Engineering, Vanung University, No. 1, Van Nung  
Rd., Chung-Li City, Taiwan

<sup>e</sup>School of Medical Laboratory Science and Biotechnology, College of Medical Science  
and Technology, Taipei Medical University, No. 250, Wuxing St., Taipei 11031, Taiwan

<sup>f</sup>Department of General Medicine, School of Medicine, College of Medicine, Taipei  
Medical University, No. 250, Wuxing St., Taipei 11031, Taiwan

<sup>g</sup>Department of Biochemistry, School of Medicine, College of Medicine, Taipei Medical  
University, No. 250, Wuxing St., Taipei 11031, Taiwan

<sup>h</sup>Biomedical Mass Imaging Research Center, Taipei Medical University, No. 250, Wuxing  
St., Taipei 11031, Taiwan

\* Corresponding author

Tel 886-2-27361661 ext. 3903; Fax 886-2-27390214; E-mail: [sylin@tmu.edu.tw](mailto:sylin@tmu.edu.tw) (S.Y.L.)

Tel 886-2-27361661 ext. 3155; Fax 886-2-27356689; E-mail: [liuyc@tmu.edu.tw](mailto:liuyc@tmu.edu.tw) (Y.C.L.)

## Abstract

Nano-structured Ag and Au with well-defined localized surface plasmon resonance (LSPR) are most popularly employed in the surface-enhanced Raman scattering (SERS)-related studies. Ag possesses the highest molar extinction coefficient in metals, resulting in stronger SERS effect than that of Au. However, compared to Au, the serious decay of SERS enhancement in ambient laboratory air limits its reliable application. In this work, we develop a new strategy for preparing highly SERS-active Ag films deposited on Au nanoparticles (NPs)-decorated SiO<sub>2</sub> mask arrays based on electrochemical methods. The idea is derived from underpotential deposition (UPD) of metals, which works on enhancing the SERS effect of underneath Au NPs as well as on reducing the decay of surface Ag films. Experimental results indicate that the SERS of Rhodamine 6G (R6G) absorbed on this developed array exhibits a higher intensity by ca. 30-fold of magnitude, as compared with that of R6G absorbed on the Au NPs-based array without the modification of Ag films. This strategy also enables it practically applicable in the trace detection of solution containing calcium pyrophosphate dihydrate (CPPD), which is a common form of calcium crystals found in articular cartilage. In addition, aging (in an atmosphere of 50% relative humidity (RH) and 20% (v/v) O<sub>2</sub> at 30 °C for 60 day) of SERS effect observed on this developed array is significantly depressed, which is comparable to that observed on the Au NPs-based array without the modification of Ag films.

## Introduction

Surface-enhanced Raman scattering (SERS) of molecules in close proximity to the surface

of nanostructured noble metals Ag and Au can be significantly enhanced by a classic factor of  $10^6$  or even higher with progress in nanotechnology.<sup>1,2</sup> For nanostructured Ag, possessing the highest molar extinction coefficient among metals,<sup>3</sup> its SERS effect is intrinsically higher than that of Au. However, compared to Au, the serious decay of SERS enhancement in ambient laboratory air limits its reliable application.<sup>4,5</sup> The known mechanism of SERS consists of two major components. One is an electromagnetic enhancements (EM),<sup>6,7</sup> resulting from an increase in the electromagnetic field at the analyte location, which is quite well recognized. The second contribution arises from charge transfer between the adsorbate–metal surface complex, which is generally referred to as the chemical enhancement (CHEM).<sup>8,9</sup> Compared to the well-recognized EM, the CHEM is poorly understood. In addition, the classic SERS enhancement of  $10^6$  orders could be understood as the product of the predominant EM enhancement of  $10^4$  orders and the lower CHEM enhancement of  $10^2$  orders. The CHEM mainly relies on self-assembled monolayers (SAMs)<sup>10,11</sup> of S- or N-containing molecules chemically adsorbed on nanostructured Ag or Au, having unique molecular selectivity. Nevertheless, the EM is widely suitable for physically adsorbed molecules on nanostructured Ag or Au in couples of nanometers.

Although created SERS effect on nanostructured Ag or Au is encouragingly huge, the reproducibility of SERS signals is equally important for its reliable application. As shown in the literature, core@shell structures<sup>12,13</sup> and array substrates<sup>14,15</sup> have emerged as promising approaches for meeting these requirements of both effective enhancement and acceptable reproducibility. However, these fabrication procedures are labor-consuming. Yang et al.<sup>16</sup> demonstrated a strategy for depositing uniform, conformal shells of Au on the surfaces of Ag nanocubes to generate Ag@Au core–shell nanocubes with greatly enhanced

chemical stability and SERS activity. Instead of conventional galvanic replacement deposition of Au on Ag, they reported a robust synthesis of Ag@Au core-shell nanocubes by directly depositing Au atoms on the surfaces of Ag nanocubes as conformal, ultrathin shells. The success of this process relies on introducing a strong reducing agent to compete with and thereby block the galvanic replacement between Ag and HAuCl<sub>4</sub>. As reported by Yang et al.,<sup>17</sup> well-ordered Au-nanorod (NR) arrays were fabricated using the focused ion beam method (denoted as fibAu\_NR). Au or Ag nanoclusters (NCs) of various sizes and dimensions were then deposited on the fibAu\_NR arrays using electron beam deposition to improve the SERS effect, which was verified using a low concentration of crystal violet (10<sup>-5</sup>M) as the probe molecule. An enhancement factor of 6.92×10<sup>8</sup> was obtained for NCsfibAu\_NR, which is attributed to the combination of intra-NC and NR localized surface plasmon resonance. When 4-aminobenzenethiol (4-ABT)-coated Au or Ag nanoparticles (NPs) were attached to NCsfibAu\_NR, the small gaps between 4-ABT-coated NPs and intra-NCs allowed detection at the single-molecule level.

Recently, we reported on an innovative and facile fabrication of Au NPs-decorated SiO<sub>2</sub> mask coated on indium tin oxide (ITO) glass as SERS array substrate.<sup>18</sup> The obtained correspondingly optimal enhancement factor (EF) is ca. 6.5 ×10<sup>7</sup> based on model probe molecules of Rhodamine 6G (R6G). In this work, a new strategy for preparing highly SERS-active Ag NPs deposited on Au NPs-decorated SiO<sub>2</sub> arrays is proposed by utilizing idea derived from underpotential deposition (UPD) metals. The advantages for improving SERS effects of high enhancement and stability are discussed. The potential application in effective detection of biochemical species of calcium pyrophosphate dihydrate (CPPD) by using the created SERS-active substrate is also investigated

## Experimental section

### Chemical reagents

Electrolytes of KCl, H<sub>2</sub>SO<sub>4</sub>, and Ag<sub>2</sub>SO<sub>4</sub>, and reagents of R6G were purchased from Acros Organics. CPPD Crystals were purchased from Sigma Organics. All of the chemical reagents were used as received without further purification. The experimental solutions were prepared by using deionized (DI) water of 18.2 MΩ cm provided from a MilliQ system.

### Sonoelectrochemical preparation of Au NPs-decorated SiO<sub>2</sub> mask

First, SiO<sub>2</sub> mask array was prepared according to a previous method.<sup>18</sup> Then Au NPs were sonoelectrochemically deposited on the prepared SiO<sub>2</sub> mask. In electrochemical experiments, a sheet of gold with bare surface area of 4 cm<sup>2</sup>, a 2 × 4 cm<sup>2</sup> platinum sheet, and KCl-saturated silver-silver chloride (Ag/AgCl) were employed as the working, counter and reference electrodes, respectively. All the electrochemical experiments were performed in a three-compartment cell at room temperature (23°C) and were controlled by a potentiostat (model PGSTAT30, Eco Chemie). In the oxidation-reduction cycle (ORC) treatment, the Au electrode was cycled in a deoxygenated 0.1 M KCl aqueous solution from -0.28 to +1.22 V vs Ag/AgCl at a rate of 500 mV/s for 200 scans under slight stirring. The durations at the cathodic and anodic vertices are 10 and 5 s, respectively. After the ORC treatment, Au- and Cl-containing complexes (precursors of Au NPs) were produced in the solution, as reported in our previous study.<sup>19</sup> Immediately, the treated Au electrode was replaced by the

prepared SiO<sub>2</sub> mask-deposited substrate with a round bare surface area of 0.238 cm<sup>2</sup> in the same solution. Then a cathodic overpotential of 0.6 V and an anodic overpotential of 0.2 V from open circuit potential (OCP) of ca. 0.81 V vs Ag/AgCl were applied in turn under sonication to prepare Au NPs-decorated SiO<sub>2</sub> mask substrate. The ratio of reaction times of cathodic deposition to anodic dissolution of Au NPs is 0.1. In applying the cathodic overpotential for pulse deposition of Au NPs, the total accumulated deposition time is 1 min. The ultrasonic treatment was performed by using an ultrasonic generator (model XL2000, Microson) and operated at 20 kHz with a barium titanate oscillator of 3.2 mm diameter to deliver a power of 80 W. The distance between the barium titanate oscillator rod and the electrode is kept at 5 mm. The prepared substrate was rinsed thoroughly with DI water for subsequent use.

#### **Preparation of Ag film-modified Au NPs-decorated SiO<sub>2</sub> mask**

The specifically cathodic deposition potentials of UPD Ag and bulk Ag deposited on the Au NPs-decorated SiO<sub>2</sub> mask substrates can be obtained from the cyclic voltammograms. The corresponding experiments were performed from -0.50 to +0.50 V versus Ag<sup>+/0</sup> at 20 mV/s in 0.1 M H<sub>2</sub>SO<sub>4</sub> aqueous solutions containing 10 mM Ag<sub>2</sub>SO<sub>4</sub>. Then the substrates were cycled in this range at 20 mV/s until the UPD Ag and bulk Ag waves became well-defined. Finally, the scan was stopped and the potential was held at 0.00 V vs Ag<sup>+/0</sup>, which is just prior to the onset of bulk Ag deposition, as discussed later, for 30 s (60 s was also used). Immediately, the Ag-deposited Au NPs-decorated SiO<sub>2</sub> mask substrates were removed and rinsed thoroughly with DI water, and finally dried in a vacuum-dryer with dark atmosphere for 1 h at room temperature for subsequent use.

### **Adsorption of probe molecules on SERS-active substrates**

In SERS measurements for R6G, 20  $\mu\text{L}$  R6G with concentration of  $2 \times 10^{-6}$  M were directly dropped on the as-prepared SERS-active substrates by using a pipette from a working solution of 100 mL. After 30 min for equilibrium the R6G-adsorbed substrates were rinsed thoroughly with deionized water to remove any unbound R6G. Finally they were dried in a dark vacuum-dryer for 1 h at room temperature for subsequent tests. In SERS measurements for CPPD,  $2 \times 10^{-5}$  M CPPD-containing solutions were sealed in cells with glass windows. The lasers were focused on the SERS-active substrates. The aging tests on the SERS-active substrates were performed in an atmosphere of 50% relative humidity (RH) and 20% (v/v)  $\text{O}_2$  at 30  $^\circ\text{C}$  for 60 days.

### **Characterization of Ag film-modified Au NPs-decorated $\text{SiO}_2$ mask**

The surface morphologies of Ag film-modified Au NPs-decorated  $\text{SiO}_2$  mask substrates were examined by scanning electron microscopy (SEM, model JEM-6500F, JEOL) with an acceleration voltage of 20 kV. For high resolution X-ray photoelectron spectroscopy (HRXPS) measurements, a ULVAC PHI Quantera SXM spectrometer with monochromatized Al  $\text{K}_\alpha$  radiation, 15 kV and 25 W, and an energy resolution of 0.1 eV was used. To avoid the interferential signals from the substrate, an arrangement of tilt  $15^\circ$  geometry between X-ray and samples was used in measurements. To compensate for surface charging effects, all HRXPS spectra are referred to the C 1s neutral carbon peak at 284.8 eV. Surface chemical compositions were determined from peak-area ratios corrected with the approximate instrument sensitivity factors. Raman spectra were recorded (Micro

Raman spectrometer, Model RAMaker) using a confocal microscope employing a diode laser operating at 785 nm. A 50x, 0.36 NA Olympus objective (with a working distance of 10 mm) was used to focus the laser light on the samples. The laser spot size was ca. 2.5  $\mu\text{m}$ . A thermoelectrically cooled Andor iDus charge-coupled device (CCD) with 1024 x 128 pixels operating at -40 °C was used as the detector with a resolution of 1  $\text{cm}^{-1}$ . All spectra were calibrated with respect to silicon wafers at 520  $\text{cm}^{-1}$ . For these measurements, a 180° geometry was used to collect the scattered radiation. A 785 nm notch filter was used to filter the excitation line from the collected light. The acquisition time for each measurement was 3 s. Three sequential measurements were made for each sample. Five replicate measurements at different areas were made to verify the spectra were a true representation of each sample. For these measurements, a spot was focused at the center of the sample; while the other four spots were focused at points ca. 1.5 mm from the center in the nominal eastern, southern, western, and northern directions. The SERS effect was evaluated on the strongest band intensity of R6G at ca. 1514  $\text{cm}^{-1}$  on the Raman spectrum. A normalized band intensity of R6G at ca. 1514  $\text{cm}^{-1}$  was obtained by subtracting this band from the nearby background of ca. 1550  $\text{cm}^{-1}$ . An average band intensity was determined from five measurements on each sample.

## **Results and discussion**

### **Au NPs-decorated SiO<sub>2</sub> arrays modified with Ag NPs**

In this work, SERS-inactive and nonconductive SiO<sub>2</sub> mask template was fabricated on conductive ITO substrate, as shown in our previous study.<sup>18</sup> The significant difference in

conductivities between bare ITO substrate and SiO<sub>2</sub> mask is very important for following sonoelectrochemical bottom-up deposition of SERS-active Au NPs in the pores of SiO<sub>2</sub> mask. The measured conductivity of prepared SiO<sub>2</sub> mask on ITO is ca.  $1.2 \times 10^2 \text{ S cm}^{-1}$ , which is ca. one-sixtieth of magnitude compared to that of ITO (ca.  $7.3 \times 10^3 \text{ S cm}^{-1}$ , which was determined by using a commercial instrument (Model RG-7B, Napson) applying a four-probe technique with a direct current (DC) measurement at room temperature.). This significant difference in conductivities guarantees the predominant bottom-up deposition of Au NPs in the pores of SiO<sub>2</sub> mask coated on the conductive ITO substrate. On the other hand, the modification of electrochemical underpotential deposition (UPD)<sup>20,21</sup> of metal atoms on metal or metal oxide surfaces is a useful method for functionalizing the surface and tailoring its properties. The UPD metal has a nobler redox potential than the corresponding bulk metal, allowing an expanded potential window in cyclic voltammetry.<sup>22</sup> As shown in our previous report,<sup>23</sup> we have created SERS-active Au NPs modified with monolayer of Ag film by using conventional UPD methods based on UPD metals deposited on flat metal substrates.<sup>24,25</sup> The improved SERS effect from the modification of UPD Ag was observed, the SERS of R6G adsorbed on the Ag UPD-modified Au NPs exhibits a higher intensity by ca. 12-fold magnitude, as compared with that of R6G adsorbed on unmodified Au NPs. In this work, strategy of UPD Ag on Au NPs-decorated SiO<sub>2</sub> arrays is modified to increase the surface coverage of Ag on Au and enhance the corresponding SERS effect. In Ag multilayers, the concentration of Ag<sub>2</sub>SO<sub>4</sub> is significantly increased in Ag multilayers from 1 to 10 mM and the scan was stopped and held at the potential of UPD Ag for a longer duration.

Figure 1 demonstrates the typical voltammetric curves obtained at  $20 \text{ mV s}^{-1}$  on

SERS-active Au NPs-decorated SiO<sub>2</sub> array in 10 mM Ag<sub>2</sub>SO<sub>4</sub> and 0.1 M H<sub>2</sub>SO<sub>4</sub>. Obviously, the waves became well-defined after three scans. In addition, the redox pairs of dissolution and deposition of bulk Ag showed at 0.043 and -0.11 V vs Ag<sup>+0</sup>, respectively. However, the potentials regarding the dissolution and deposition of UPD Ag on the Au NPs-decorated SiO<sub>2</sub> array did not show clearly due to monolayer of UPD Ag on porous Au NPs are hard recorded. Therefore, in this work, the Au NPs-decorated SiO<sub>2</sub> arrays were cycled in this range at 20 mV/s until the UPD Ag and bulk Ag waves became well-defined. For Ag multilayers, the scan was stopped and the potential was held at 0.00 V vs Ag<sup>+0</sup>, which is just prior to the onset of bulk Ag deposition, for different durations.

Figure 2 shows the surface morphology of a fabricated SiO<sub>2</sub> mask and the SiO<sub>2</sub> masks decorated with different NPs of Au and Ag. As shown in Fig. 2a, pore sizes of ca. 350 nm with wall thicknesses of ca. 60 nm were observed on the SiO<sub>2</sub> mask. As demonstrated in Fig. 2b for deposition of Au NPs on the SiO<sub>2</sub> mask for 1 min by using pulsed sonoelectrochemical method, the Au NPs are basically electrodeposited in the pores of SiO<sub>2</sub> mask, as expected. Fig. 2c shows the deposition of bulk Ag on the Au NPs-decorated SiO<sub>2</sub> mask. Obviously, over Ag NPs were deposited both on the Au NPs in the pore of SiO<sub>2</sub> mask and the walls of SiO<sub>2</sub> mask. These results would reduce the effect of Ag multilayers and the reproducibility of SERS-active array. Fig. 2d shows the deposition of Ag multilayers on the Au NPs-decorated SiO<sub>2</sub> array for 30 s. Clearly, most of the Ag NPs were deposited on the Au NPs in the pore of SiO<sub>2</sub> mask, which would increase the reproducibility of SERS-active array based on laser spot size of 2.5 μm. Also, the surface morphology shows typical aspects of rough surfaces with strong Raman activities, which demonstrate microstructures smaller than 100 nm.<sup>26,27</sup> On the Ag multilayers -modified Au NPs-decorated SiO<sub>2</sub> mask, the SERS effects are expected to be stronger than those

observed on the unmodified Au NPs because both Ag and Au NPs contribute to the total SERS effects under laser irradiation. The Ag multilayers can directly create electromagnetic enhancement, while the underneath Au NPs can also contribute to the total SERS effects due to the long-range effect of electromagnetic enhancement of the irradiated Ag multilayers, as reported in the literature.<sup>28,29</sup> With increasing the deposition time of Ag multilayers from 30 to 60 s, bigger particle sizes of Ag NPs can be observed, as shown in Fig. 2e. In SERS effect, molecules located between two metallic NPs display the greatest SERS enhancement,<sup>30,31</sup> this kind of microstructure provides less chance for probe molecules adsorbed on two metallic NPs. Therefore, a weaker SERS effect is expected for longer deposition of Ag multilayers, as discussed later.

The existence of deposited Ag multilayers on Au NPs was further examined by using HRXPS analyses. Curves a, b and c of Fig. 3 exhibit the HRXPS Ag  $3d_{5/2-3/2}$  core-level spectra of bulk Ag and Ag multilayers deposited on Au NPs-decorated  $\text{SiO}_2$  arrays for 30 and 60 s, respectively. As reported by Jennings and Laibinis,<sup>22</sup> the binding energy of UPD Ag deposited on flat polycrystalline Au is lower than that of the corresponding bulk Ag by 0.6 eV. However, when Fig. 3b (deposition of Ag multilayers for 30 s) is inspected and compared with Fig. 3a (bulk Ag), the Ag  $3d_{5/2}$  main peak of the Ag multilayers is located at 368.3 eV with a positive shift of 0.3 eV with respect to that of bulk Ag. The difference can be ascribed to the fact that the Ag multilayers are deposited onto Au NPs in this study, not on a flat polycrystalline Au. A charge transfer occurs from Ag multilayers to the Au NPs. It results in a stronger interaction between them. Clearly, the Ag multilayers deposited on the Au NPs-decorated  $\text{SiO}_2$  array in this study is well-defined. It shows in a type of valence Ag. With increasing the deposition time of Ag multilayers from 30 to 60 s, the Ag  $3d_{5/2}$  main peak of the Ag multilayers is located at 368.2 eV with a less positive shift of 0.2 eV with

respect to that of bulk Ag. It suggests a reduced interaction between Ag multilayers and Au NPs, as shown in Fig. 3c. Therefore, we suggest that the Ag multilayers deposited on Au NPs are of valence Ag due to charge transfers from Ag multilayers to the Au NPs. This type of Ag multilayers is not prone to oxidation in air, resulting in the deposited Ag multilayers are stable in air, which will be confirmed in the aging test. Also, the coupling between the Au NPs and the Ag multilayers indeed happen. Further HRXPS analyses on Ag and Au indicate that the contents of Ag multilayers on Ag multilayers-modified Au NPs-decorated SiO<sub>2</sub> arrays are about 74 and 88 mol % for holding the potential at 0.00 V versus Ag<sup>+/0</sup> for 30 and 60 s in preparation, respectively. These values are calculated from the ratios of content of Ag to contents of Ag and Au. Other elements are not considered in analyses. The obtained values of 73 and 88 mol % from HRXPS analyses can represent coverages of Ag multilayers deposited on Au NPs, which were also used in the literature.<sup>22,32</sup> Compared to conventional deposition of UPD Ag, these results confirm that deposition of Ag multilayers with high coverage on the Au NPs-decorated SiO<sub>2</sub> arrays can be obtained by increasing the concentration of Ag salt and prolonging the cathodic polarization time in preparation.

### **SERS performances on Au NPs-decorated SiO<sub>2</sub> arrays modified with Ag NPs**

Figure 4 shows the Raman spectra of  $2 \times 10^{-6}$  M R6G adsorbed on SERS-inactive SiO<sub>2</sub> mask and the SiO<sub>2</sub> masks decorated with different NPs of Au and Ag. As shown in spectrum a of Fig. 4, it is featureless due to lack of SERS effect from SiO<sub>2</sub> mask. With the decoration of SERS-active Au NPs on SiO<sub>2</sub> mask, the characteristic Raman spectrum of R6G is demonstrated, as shown in spectrum b of Fig. 4. With the modification of bulk Ag

on the Au NPs-decorated SiO<sub>2</sub> array, this characteristic Raman intensity of R6G is increased by ca. 5-fold of magnitude, as shown in spectrum c of Fig. 4. Encouragingly, as shown in spectrum d of Fig. 4 for the modification of Ag multilayers (deposition for 30 s) on the Au NPs-decorated SiO<sub>2</sub> array, this intensity is significantly increased by ca. 30-fold of magnitude, as compared with that for Au NPs-decorated SiO<sub>2</sub> array. With increasing the deposition time of Ag multilayers from 30 to 60 s, this increase in intensity is reduced to ca. 10-fold of magnitude, as shown in spectrum e of Fig. 4. In calculating the relative intensity, we employ the normalized Raman intensity, which is calculated from the ratio of the strongest intensity of R6G adsorbed on different types of Ag-modified Au NPs-decorated SiO<sub>2</sub> arrays to that of R6G adsorbed on Au NPs-decorated SiO<sub>2</sub> array. Thus, no correction to the normal Raman scattering intensity is necessary to account for differences in sampling geometry and scattering phenomena.<sup>33</sup> As shown in spectrum d of Fig. 4 for the modification of Ag multilayers (deposition for 30 s), it is characteristic of Raman spectrum of R6G.<sup>34-36</sup> The band at ca. 614 cm<sup>-1</sup> is assigned to the C-C-C ring in-plane vibration mode. The band at ca. 776 cm<sup>-1</sup> is assigned to the C-H out-of-plane bend mode. The bands at ca. 1130 and 1185 cm<sup>-1</sup> are assigned to the C-H in-plane bend modes. The bands at ca. 1314 and 1579 cm<sup>-1</sup> are assigned to the N-H in-plane bend modes. The bands at ca. 1365, 1514 and 1652 cm<sup>-1</sup> are assigned to the C-C stretching modes. In addition, the Ag multilayers (deposition for 30 s)-modified Au NPs-decorated SiO<sub>2</sub> array exhibits a large enhancement factor (EF) of 4.3 × 10<sup>8</sup>. The EF value is calculated from the definition in the literature,<sup>37</sup> which is shown as below.

$$G=(N_2/N_1) \times (I_{\text{SERS}}/I_{\text{ref}}) \quad (1)$$

where  $I_{\text{SERS}}$  is the integrated intensity of the R6G band under consideration collected on the substrate surface.  $I_{\text{ref}}$  is the integrated intensity of the same Raman band obtained by focusing the laser line on an ITO substrate immersed in a  $2 \times 10^{-3}$  M R6G solution. Based on this concentration of  $2 \times 10^{-3}$  M the normal Raman spectroscopy of R6G is acceptable.  $N_1$  is the number of molecules constituting the first monolayer adsorbed on the substrate surface under the laser spot area. Because the real surface area of Ag multilayers-modified Au NPs-decorated  $\text{SiO}_2$  array is difficultly obtained collection area based on laser spot size ( $6.25 \mu\text{m}^2$ ) was used instead to calculate  $N_1$  (collection area divided by the surface area of one R6G molecule). In the calculation, the surface area of one R6G molecule of  $2 \times 10^{-18} \text{m}^2/\text{molecule}$  was used.<sup>38</sup> This value was calculated from the geometric area of length (1.37 nm)  $\times$  width (1.43 nm) of one R6G molecule. Thus, the estimated value for  $N_1$  is ca.  $3.125 \times 10^6$ .  $N_2$  is the number of molecules excited within the volume of the laser waist for the  $2 \times 10^{-3}$  M R6G solution. In calculating  $N_2$  (irradiated solution volume multiplied by the concentration of analyzed molecule) the volume of the laser waist is approximately to a cylinder with a radius of  $50 \mu\text{m}$  and a depth in the sample of 3 mm. The calculated volume is ca.  $9.5 \times 10^{-12} \text{m}^3$ . Thus, the estimated value for  $N_2$  is ca.  $11.3 \times 10^{12}$ . Based on the ratio of ( $I_{\text{SERS}}/I_{\text{ref}}$ ) being  $1.2 \times 10^2$  calculated from the Raman intensities at ca.  $1514 \text{cm}^{-1}$ , the proposed SERS-active substrate of Ag multilayers-modified Au NPs-decorated  $\text{SiO}_2$  array exhibits a large EF of  $4.3 \times 10^8$ . Moreover, relative standard deviation (RSD) based on the strongest band intensity of R6G at ca.  $1514 \text{cm}^{-1}$  was calculated from the five spots on different areas for the same sample. The calculated values of RSD are ca. 18 and 16 % for Au NPs-decorated  $\text{SiO}_2$  arrays modified with Ag multilayers for depositions of 30 and 60 s,

respectively. As reported by Huang et al.,<sup>39</sup> SERS substrate of ordered Ag/Si nanowires array with RSD of 14 % and EF of  $\sim 10^6$  was presented. As reported by Li et al.,<sup>40</sup> SERS substrate of ordered Au semishells on hollow on TiO<sub>2</sub> spheres array with RSD of 12 % and EF of  $1.4 \times 10^5$  was presented. In SERS studies, high SERS enhancement is generally accompanied with poor reproducibility. In this work, the large EF observed in this system is more compatible in SERS application although the RSD is slightly higher than those shown in the literature.

For practical application, the developed SERS-active substrate was also examined in biomedical detections. Conventionally, light microscopy is capable of detecting disease-related crystals seen in gouty arthritis.<sup>41</sup> Recently, Raman spectroscopy was employed for detecting this CPPD crystal because their unique Raman shift spectral pattern and little interference from water.<sup>41-43</sup> However, the detection of CPPD by using SERS technique was less shown in the literature. Fig. 5 demonstrates the corresponding SERS spectra of  $2 \times 10^{-5}$  M CPPD adsorbed on different types of Ag and Au NPs-decorated SiO<sub>2</sub> arrays. Spectrum a of Fig. 5 represents the solid CPPD crystals for reference. The characteristic Raman bands of CPPD at ca. 741, 968, 1051, 1143, 1245, 1366 and 1885 cm<sup>-1</sup> are basically consistent with those of CPPD crystals reported in the literature.<sup>41-43</sup> As shown in spectrum b of Fig. 5 for Au NPs-decorated SiO<sub>2</sub> array without the modification of Ag multilayers, the spectrum provides less information on the presence of slightly dissolved CPPD. With the modification of Ag multilayers (deposition for 30 s) on Au NPs-decorated SiO<sub>2</sub> array, in it was clearly found that the spectral intensity can be effectively enhanced by ca. 6-fold of magnitude (based on the strongest and unique Raman band at 1051 cm<sup>-1</sup>) due

to the contribution from the Ag multilayers, as comparing spectrum c with spectrum b in Fig. 5.

It is well known that, Ag NPs as compared to Au NPs were severe susceptibility to oxidation under atmospheric condition.<sup>4,5,44,45</sup> Therefore, their stabilities on the corresponding SERS effects for Au NPs-deposited SiO<sub>2</sub> array and Ag film-modified Au NPs-deposited SiO<sub>2</sub> array (developed in this work for the strongest SERS effect) were examined in an atmosphere of 50% RH and 20% (v/v) O<sub>2</sub> at 30 °C for 60 days. Fig. 6 shows the corresponding decays of the SERS enhancement capabilities as a function of aging time. The relative intensity was calculated as before. Obviously, the SERS enhancement capabilities were gradually decreased with time for both arrays. After 60 days, 58% of the intensity remained for the Au NPs-deposited SiO<sub>2</sub> array without the modification of Ag multilayers. Interestingly, comparable 52% of the intensity remained for the Ag film-modified Au NPs-deposited SiO<sub>2</sub> array developed in this work. Conclusively, significant improvement in anti-aging of SERS-active substrate is successfully achieved by using Ag multilayers deposited on Au NPs-deposited SiO<sub>2</sub> array with a considerable coverage of 73 mol % of Ag on Au.

## Conclusion

In this work, we have developed an innovative and facile preparation of SERS-active ordered array of Ag multilayers-modified Au NPs-deposited SiO<sub>2</sub> mask coated on ITO glass. By increasing the concentration of Ag<sub>2</sub>SO<sub>4</sub> and prolonging the duration in Ag multilayers, the coverage of Ag on Au can be significantly increased. This results in the corresponding enhancement of SERS effect as well as in reducing the decay of surface Ag films. Experimental results indicate that the SERS of R6G absorbed on this developed array exhibits a higher intensity by ca. 30-fold of magnitude, as compared with that of R6G absorbed on the Au NPs-based array without the modification of Ag films. This strategy also enables it practically applicable in the trace detection of solution containing CPPD. In addition, aging tests suggest that SERS effect observed on this developed array is significantly depressed, which is comparable to that observed on the Au NPs-based array without the modification of Ag films. In addition, the large EF and acceptable RSD observed in this system is more compatible in SERS application. Further studies for obtaining optimal both low RSD and large based on this strategy are underway.

## Acknowledgments

The authors thank Taipei Medical University and Taipei Medical University Hospital for their financial support (Taipei Medical University-Taipei Medical University Hospital Joint Research Program; 103TMU – TMUH – 01).

## References

- 1 S. Huang, X. Ling, L. Liang, Y. Song, W. Fang, J. Zhang, J. Kong, V. Meunier and M. S. Dresselhaus, *Nano Lett.*, 2015, **15**, 2892.
- 2 F. D. Mai, T. C. Hsu, Y. C. Liu, K. H. Yang and B. C. Chen, *Chem. Commun.*, 2011, **47**, 2958.
- 3 T. A. Taton, C. A. Mirkin and R. L. Letsinger, *Science*, 2000, **289**, 1757.
- 4 N. L. Rosi and C. A. Mirkin, *Chem. Rev.*, 2005, **105**, 1562.
- 5 K. H. Yang, Y. C. Liu, T. C. Hsu and M. Y. Juang, *J. Mater. Chem.*, 2010, **20**, 7530.
- 6 E. Hesse and J. A. Creighton, *Langmuir*, 1999, **15**, 3545.
- 7 K. Wu, T. Rindzevicius, M. S. Schmidt, K. B. Mogensen, A. Hakonen and A. Boisen, *J. Phys. Chem. C*, 2015, **119**, 2053.
- 8 R. P. Van Duyne, J. C. Hulteen and D. A. Triechel, *J. Chem. Phys.*, 1993, **99**, 2101.
- 9 Y. C. Liu, K. H. Yang and T. C. Hsu, *Anal. Chim. Acta*, 2009, **636**, 13.
- 10 Z. L. Yu, J. Casanova-Moreno, I. Guryanov, F. Maran and Dan Bizzotto, *J. Am. Chem. Soc.*, 2015, **137**, 276.
- 11 R. G. Nuzzo, F. A. Fusco and D. L. Allara, *J. Am. Chem. Soc.*, 1987, **109**, 2358.
- 12 J. F. Li, Y. F. Huang, Y. Ding, Z. L. Yang, S. B. Li, X. S. Zhou, F. R. Fan, W. Zhang, Z. Y. Zhou, D. Y. Wu, *et al.*, *Nature* 2010, **464**, 392.
- 13 M. Lin, Y. Wang, X. Sun, W. Wang and L. Chen, *ACS Appl. Mater. Interfaces*, 2015, **7**, 7516.
- 14 Y. Lina, J. Liao, M. Yang and C. Wu, *Biosens. Bioelectr.*, 2012, **35**, 447.
- 15 G. Kang, A. Matikainen, P. Stenberg, E. Färm, P. Li, M. Ritala, P. Vahimaa, S.

- Honkanen and X. Tan, *ACS Appl. Mater. Interfaces*, 2015, **7**, 11452.
- 16 Y. Yang, J. Liu, Z. W. Fu and D. Qin, *J. Am. Chem. Soc.*, 2014, **136**, 8153.
- 17 K. Sivashanmugan, J. D. Liao, P. L. Shao, B. H. Liu, T. Y. and C. Y. Chang, *Biosens. Bioelectr.*, 2015, **72**, 61.
- 18 L. Y. Chen, K. H. Yang, H. C. Chen, Y. C. Liu, C. H. Chen, Q. Y. Chen, *Analyst*, 2014, **139**, 1929.
- 19 Y. C. Liu, *Langmuir*, 2002, **18**, 174.
- 20 Y. Grunder, P. Thompson, A. Brownrigg, M. Darlington, C.A. Lucas, *J. Phys. Chem. C*, 2012, **116**, 6288.
- 21 D. Oyamatsu, M. Nishizawa, S. Kuwabata and H. Yoneyama, *Langmuir*, 1998, **14**, 3302.
- 22 G. K. Jennings and P. E. Laibinis, *J. Am. Chem. Soc.*, 1997, **119**, 5208.
- 23 C. C. Chang, K. H. Yang, Y. C. Liu, C. C. Yu and Y. H. Wu, *Analyst*, 2012, **137**, 4950.
- 24 K. Ogaki and K. Itaya, *Electrochim. Acta*, 1995, **40**, 1257.
- 25 S. Takami, G. K. Jennings and P. E. Laibinis, *Langmuir*, 2001, **17**, 448.
- 26 G. Cardini, M. Maurizio-Miranda and V. Schettino, *J. Phys. Chem. B*, 2004, **108**, 17007.
- 27 E. Hesse and J. A. Creighton, *Langmuir*, 1999, **15**, 3545.
- 28 W. Song, Y. Wang and B. Zhao, *J. Phys. Chem. C*, 2007, **111**, 12786.
- 29 A. Zwijnenburg, A. Goossens, W. G. Sloof, M. W. J. Craje, A. M. Kraan, L. J. Jongh, M. Makkee and J. A. Moulijn, *J. Phys. Chem. B*, 2002, **106**, 9853.
- 30 N. Liver, A. Nitzan and J. Gersten, *Chem. Phys. Lett.*, 1984, **111**, 449.
- 31 M. Xu and M. J. Dignam, *J. Chem. Phys.*, 1994, **100**, 197.

- 32 D. Oyamatsu, M. Nishizawa, S. Kuwabata and H. Yoneyama, *Langmuir*, 1998, **14**, 3302.
- 33 C. E. Taylor, J. E. Pemberton, G. G. Goodman and M. H. Schoenfish, *Appl. Spectrosc.*, 1999, **53**, 1212.
- 34 Y. Lu, G. L. Liu and L. P. Lee, *Nano Lett.*, 2005, **5**, 5.
- 35 Z. Sun, Y. Li, Y. Wang, X. Chen, J. Zhang, K. Zhang, Z. Wang, C. Bao, J. Zeng, B. Zhao and B. Yang, *Langmuir*, 2007, **23**, 10725.
- 36 L. Jensen and G. C. Schatz, *J. Phys. Chem. A*, 2006, **110**, 5973.
- 37 N. Felidj, J. Aubard, G. Levi, J. R. Krenn, M. Salerno, G. Schider, B. Lamprecht, A. Leitner and F. R. Aussenegg, *Phys. Rev. B*, 2002, **65**, 075419.
- 38 N. Tsurumachi, H. Okamoto, K. Ishii, H. Kohkami, S. Nakanishi, T. Ishii, N. Takahashi, C. Dou, P. Wen and Q. Feng, *J. Photoch. Photobio. A*, 2012, **243**, 1.
- 39 J. Huang, Y. Zhao, X. Zhang, L. He, T. Wong, Y. Chui, W. Zhang and S. Lee, *Nano Lett.*, 2013, **13**, 5039.
- 40 X. Li, H. Hu, D. Li, Z. Shen, Q. Xiong, S. Li and H. J. Fan, *ACS Appl. Mater. Interfaces*, 2012, **4**, 2180.
- 41 P. MacMullan, G. McMahon and G. McCarthy, *Joint Bone Spine*, 2011, **78**, 363.
- 42 X. Cheng, D.G. Haggins, R.H. York, Y.N. Yeni and O. Akkus, *Appl. Spectrosc.*, 2009, **63**, 386.
- 43 A. Yavorsky, A.H. Santana, G. McCarthy and G. McMahon, *Analyst*, 2008, **133**, 318
- 44 C. Shankar, A. T. N. Dao, P. Singh, K. Higashimine, D. M. Mott and S. Maenosono, *Nanotechnology*, 2012, **23**, 245704.

45 M. D. McMahon, R. Lopez, H. M. Meyer III, L. C. Feldman and R. F. Haglund JR, *Appl.*

*Phys. B*, 2005, **80**, 921.

### Figure Captions

Fig. 1. Cyclic voltammograms of the first, second, third and fourth scans for UPD Ag on Au nanoparticle-decorated SiO<sub>2</sub> mask at 20 mV/s in 0.1 M H<sub>2</sub>SO<sub>4</sub> aqueous solutions containing 10 mM Ag<sub>2</sub>SO<sub>4</sub>.

Fig. 2. SEM images of different Ag film-modified Au NPs sonoelectrodeposited on SiO<sub>2</sub> masks: (a) blank SiO<sub>2</sub> mask (without deposition of metal NPs); (b) deposition of Au NPs (without further deposition of Ag films); (c) Ag films deposited on Au NPs (potential held at -0.11 vs Ag<sup>+/0</sup>, corresponding to bulk deposition, and electrode taken out from solution immediately); (d) Ag films deposited on Au NPs (potential held at 0.00 vs Ag<sup>+/0</sup>, corresponding to UPD, for 30 s); (e) Ag films deposited on Au NPs (potential held at 0.00 vs Ag<sup>+/0</sup>, corresponding to UPD, for 60 s).

Fig. 3. HRXPS Ag 3d<sub>5/2-3/2</sub> core-level spectra of different Ag films deposited on Au nanoparticle-decorated SiO<sub>2</sub> masks: (a) bulk Ag; (b) Ag multilayers for 30 s; (c) Ag multilayers for 60 s.

Fig. 4. Raman spectra of 2 × 10<sup>-6</sup> M R6G adsorbed on different Ag film-modified Au NPs sonoelectrodeposited on SiO<sub>2</sub> masks: (a) blank SiO<sub>2</sub> mask (without deposition of metal NPs); (b) Au NPs without further deposition of Ag films; (c) Ag films deposited on Au NPs (potential held at -0.11 vs Ag<sup>+/0</sup>, corresponding to bulk deposition, and electrode taken out from solution immediately); (d) Ag films deposited on Au NPs (potential held at 0.00 vs Ag<sup>+/0</sup>, corresponding to UPD, for 30 s); (e) Ag films deposited on Au NPs (potential held at 0.00 vs Ag<sup>+/0</sup>, corresponding to UPD, for 60 s).

Fig. 5. Raman spectrum of CPPD crystals (a), SERS spectra of 2 × 10<sup>-5</sup> M CPPD adsorbed

on Au NPs (without further deposition of Ag films) sonoelectrodeposited on SiO<sub>2</sub> mask (b) and on Ag films (potential held at 0.00 vs Ag<sup>+/0</sup>, corresponding to UPD, for 30 s) deposited on Au NPs sonoelectrodeposited on SiO<sub>2</sub> mask (c).

Fig. 6. Variation of normalized Raman intensity of R6G adsorbed on different substrates in 50% RH and 20% (v/v) O<sub>2</sub> at 30 °C for 60 days. Solid and open circles represent R6G adsorbed on Au NPs-deposited SiO<sub>2</sub> mask (without further deposition of Ag films) and on Ag film-modified Au NPs-deposited SiO<sub>2</sub> mask (developed in this work for the strongest SERS effect), respectively.

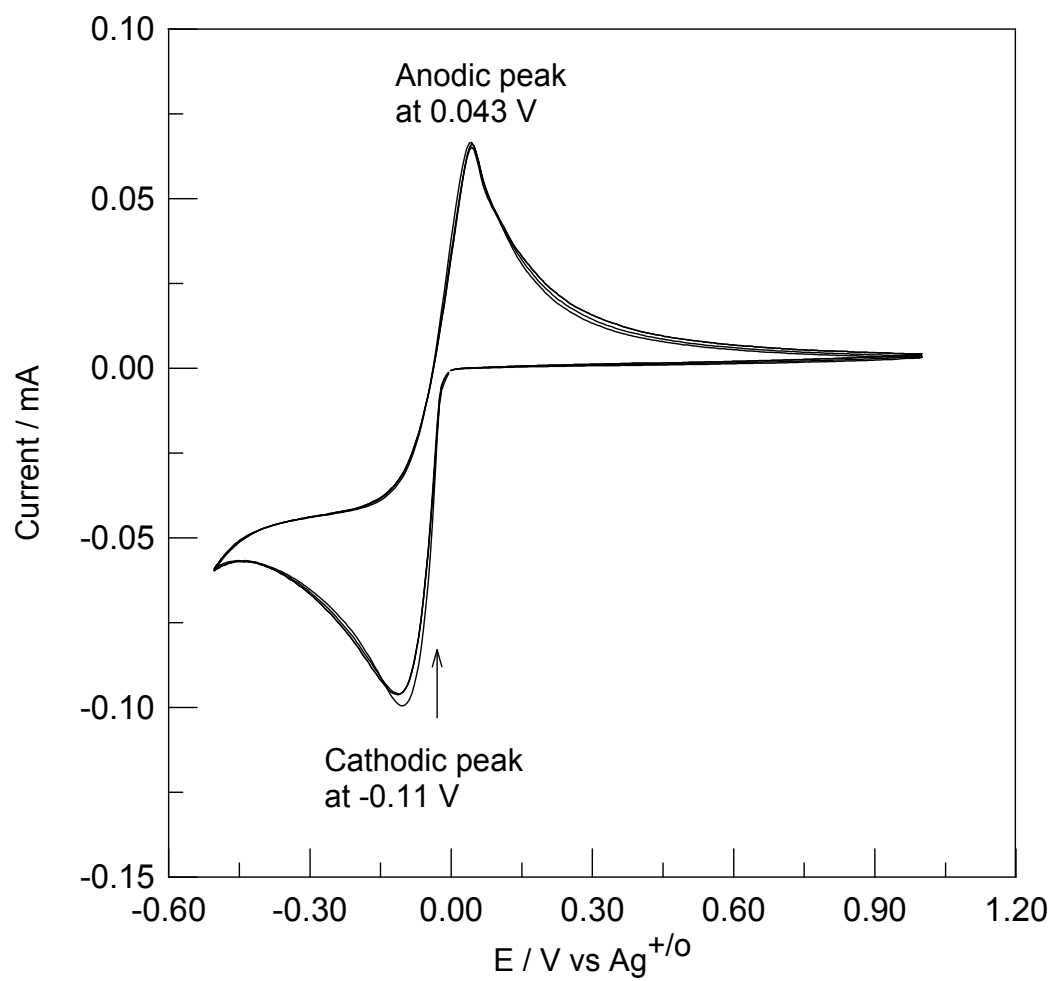
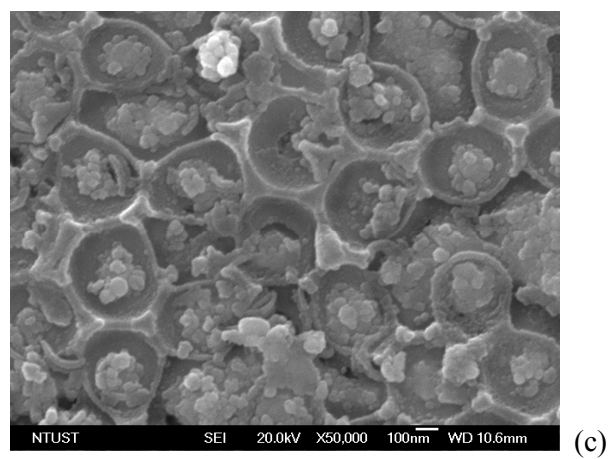
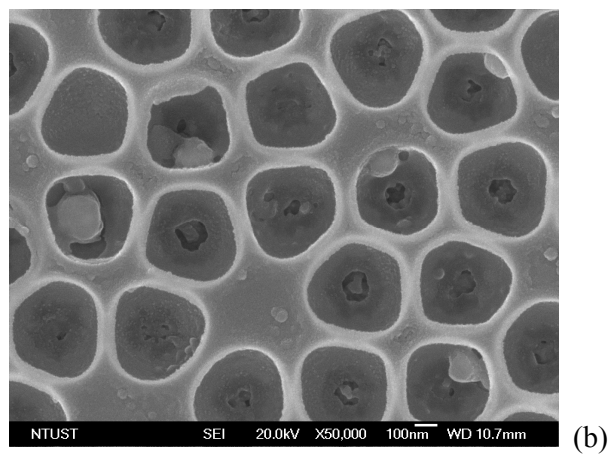
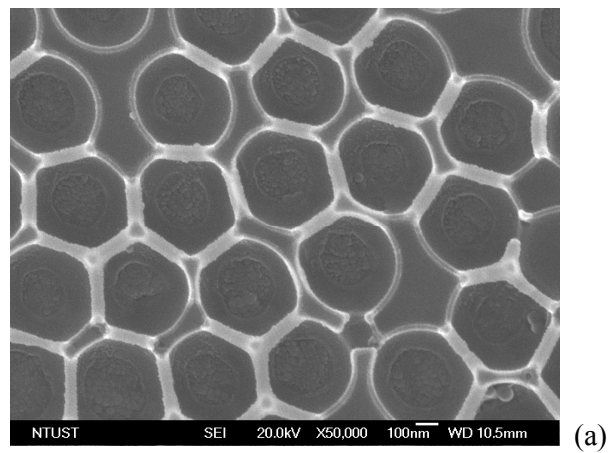


Fig. 1.



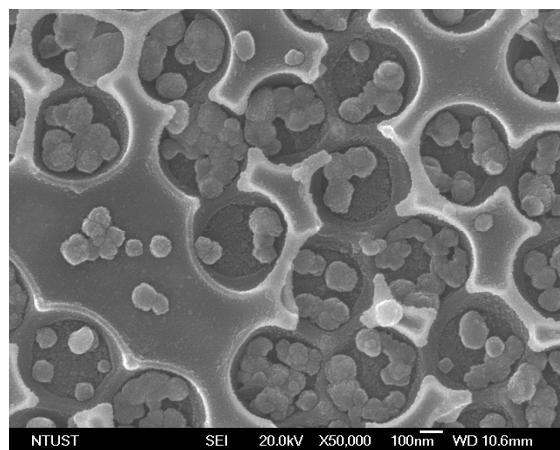
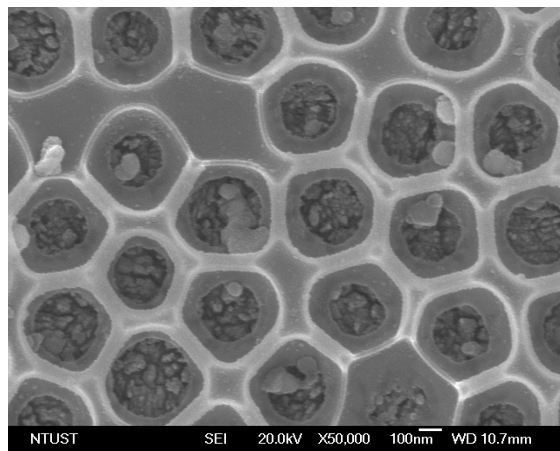


Fig. 2.

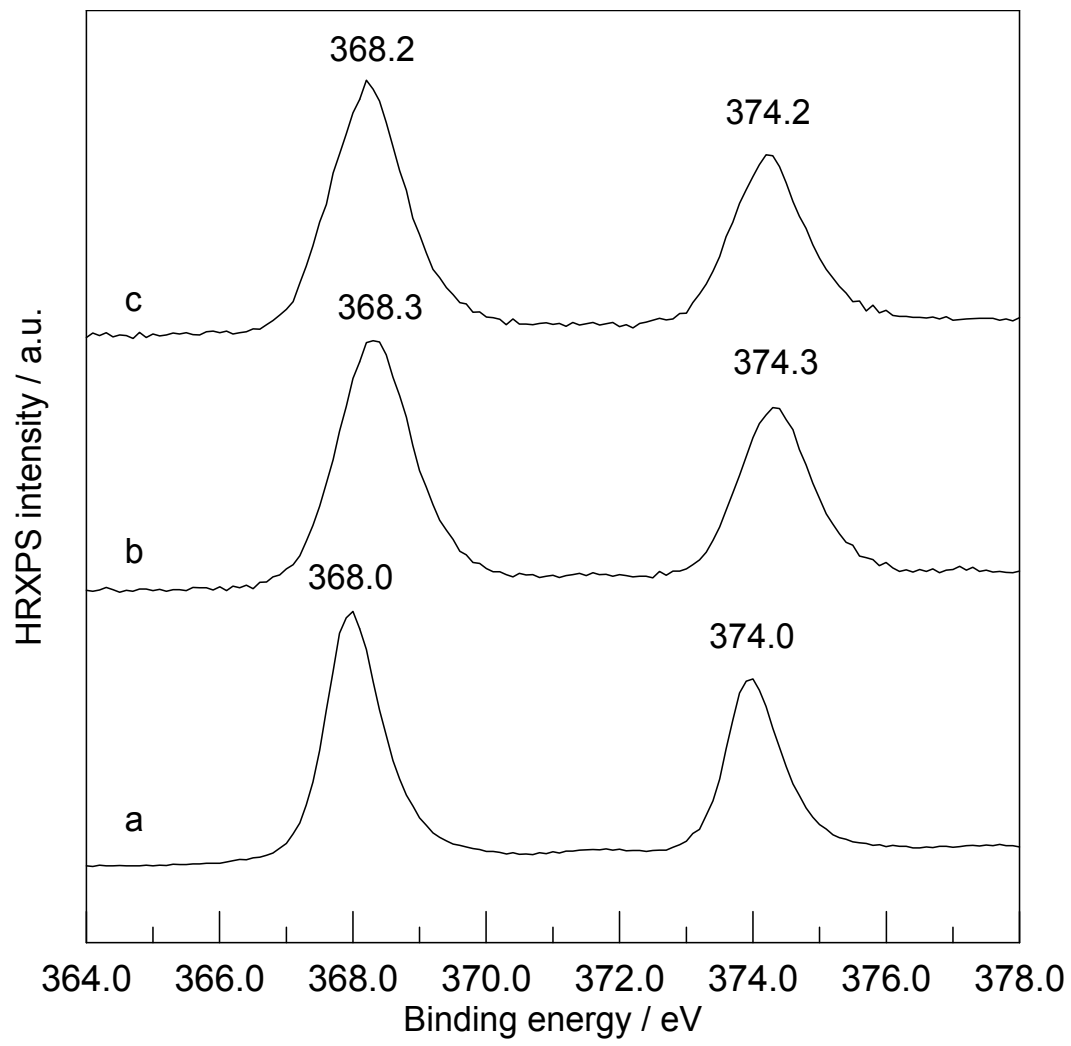


Fig. 3.

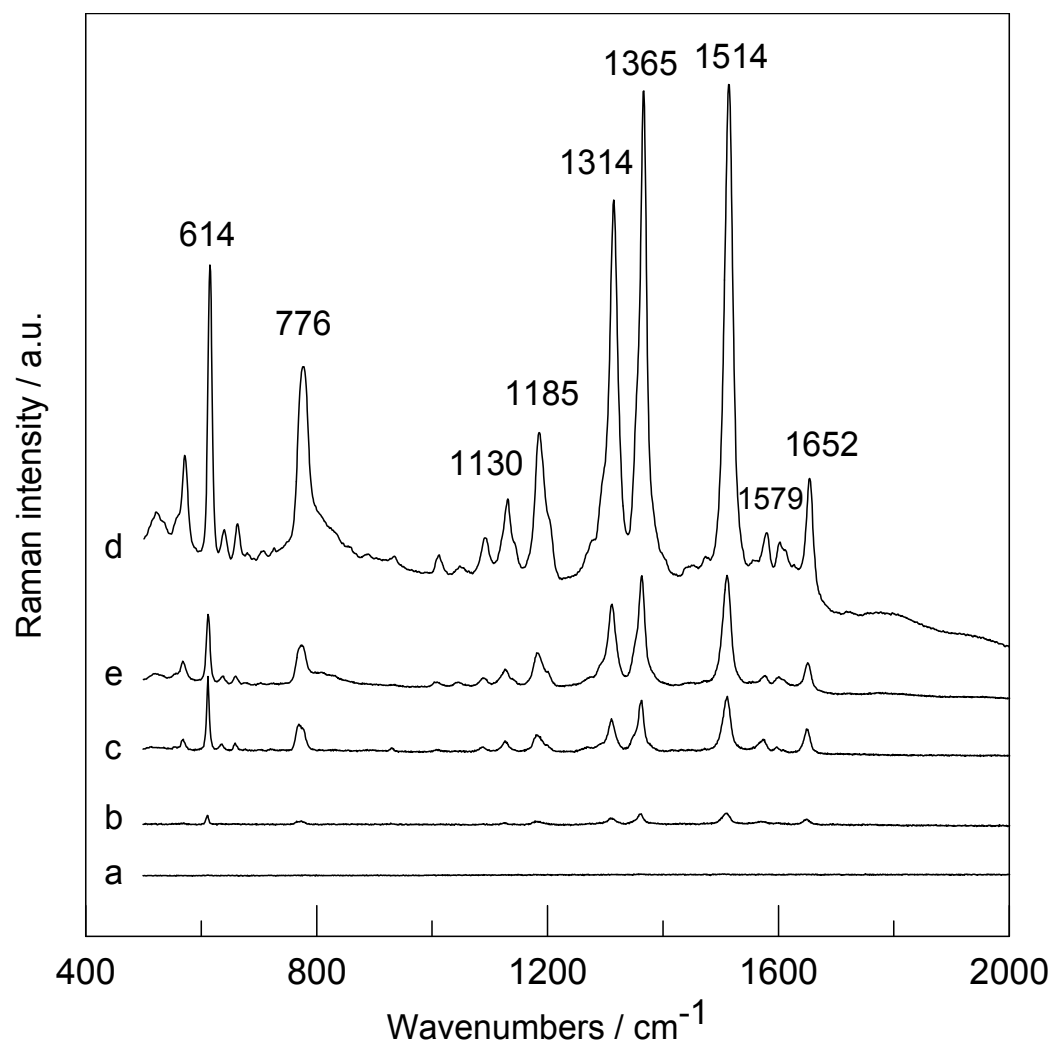


Fig. 4.

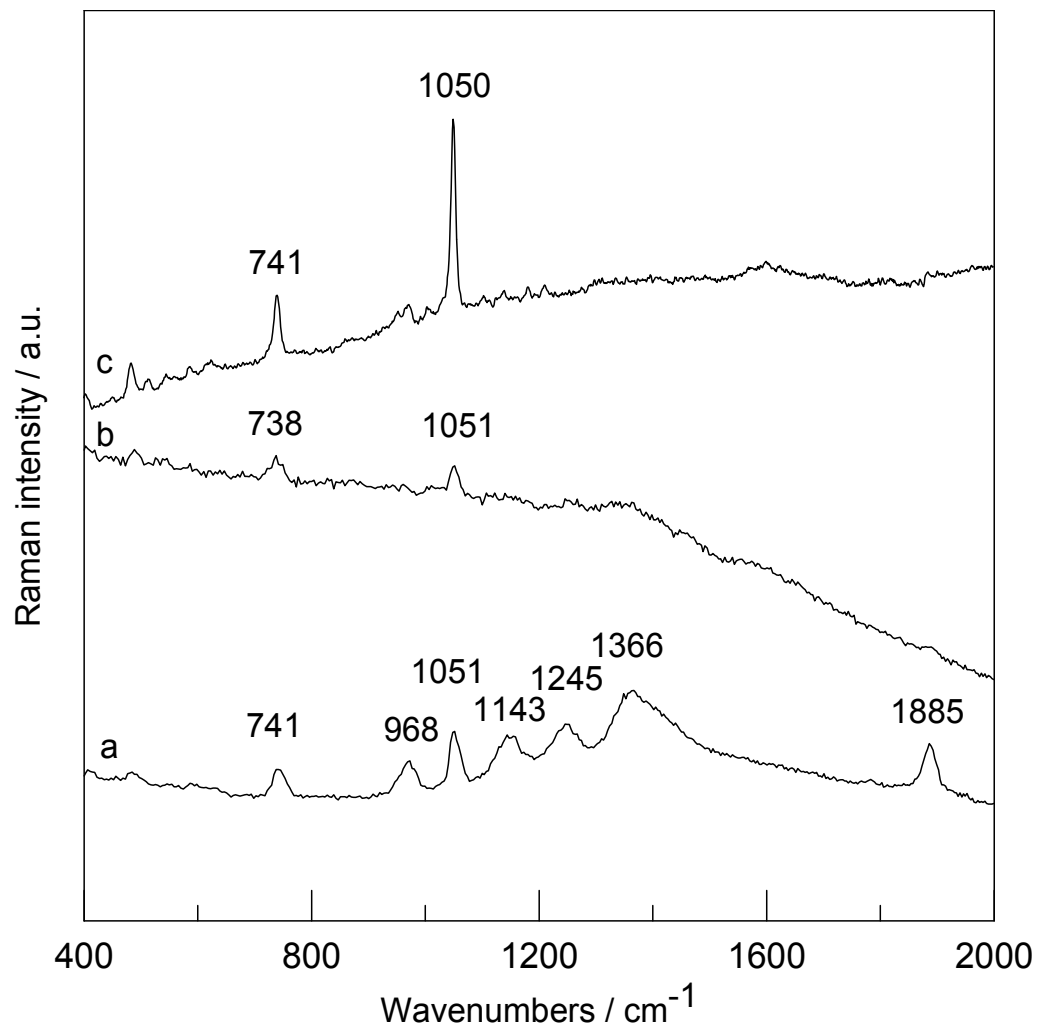


Fig. 5.

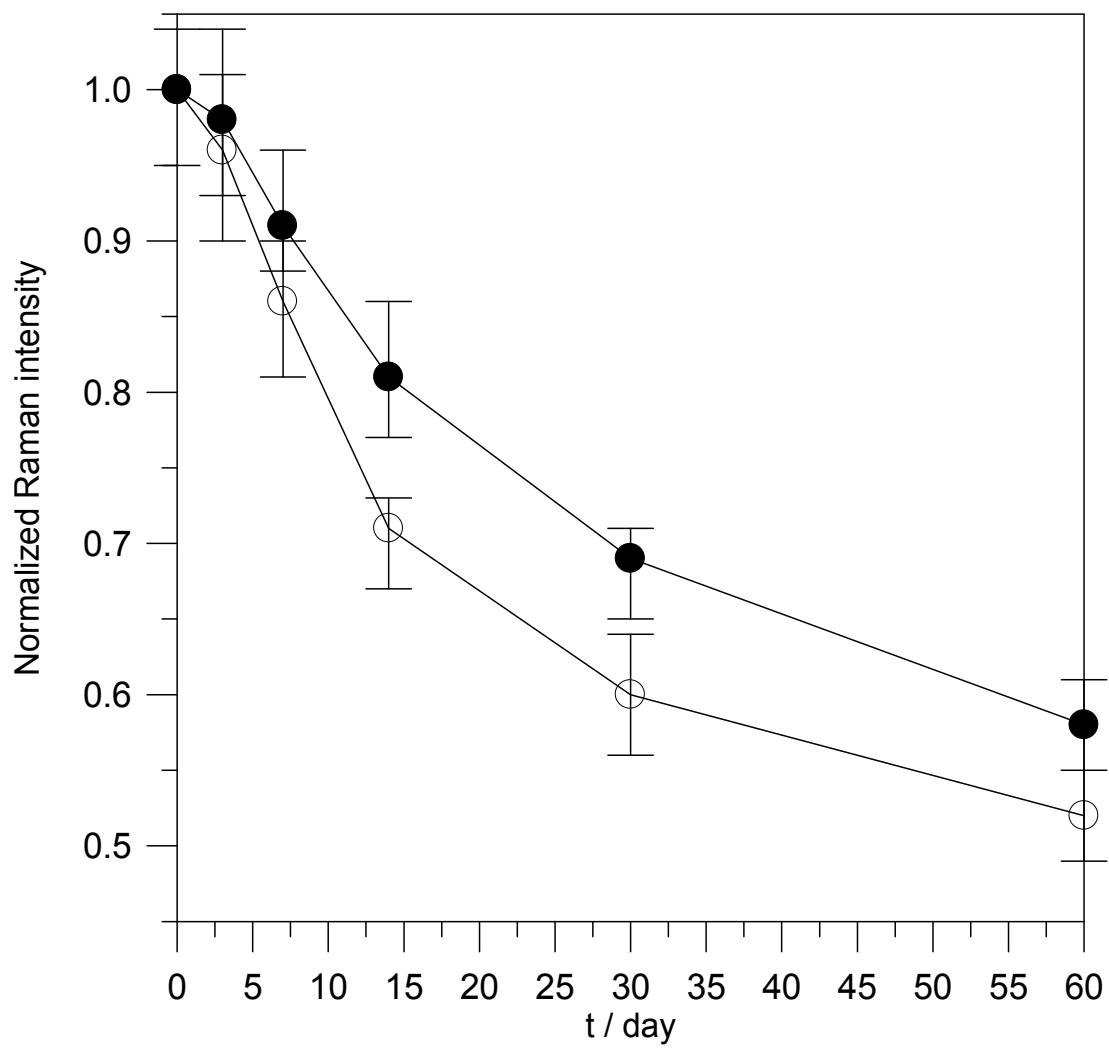


Fig. 6